PAPER *Special Issue on Machine Vision Applications*

Robust Method for Recovering Sign of Gaussian Curvature from Multiple Shading Images

Shinji FUKUI[†], **Yuji IWAHORI**[†], ***Regular Members***, **Robert J. WOODHAM**[††], ***Nonmember***, **Kenji FUNAHASHI**[†], ***and*** **Akira IWATA**[†], ***Regular Members***

SUMMARY This paper proposes a new method to recover the sign of local Gaussian curvature from multiple (more than three) shading images. The information required to recover the sign of Gaussian curvature is obtained by applying Principal Components Analysis (PCA) to the normalized irradiance measurements. The sign of the Gaussian curvature is recovered based on the relative orientation of measurements obtained on a local five point test pattern to those in the 2-D subspace called the eigen plane. Using multiple shading images gives a more accurate and robust result and minimizes the effect of shadows by allowing a larger area of the visible surface to be analyzed compared to methods using only three shading images. Furthermore, it allows the method to be applied to specular surfaces. Since PCA removes linear correlation among images, the method can produce results of high quality even when the light source directions are not widely dispersed.

key words: *Gaussian curvature, shape representation and recovery, physics-based vision, principal components analysis*

1. Introduction

Surface curvature is one descriptor of the local shape of a 3-dimensional object. Surface curvature is a viewpoint invariant shape descriptor. Thus, in computer vision, it potentially is useful for many tasks including shape recovery, shape modeling, segmentation, object recognition, scene analysis and pose determination.

Woodham [1] extended photometric stereo to estimate both the local surface gradient and the local surface curvature. The method uses three images acquired under different conditions of illumination. The method is empirical in that reflectance is estimated using a calibration object of known shape. No specific assumptions about surface reflectance or light source directions need to be made. On the other hand, the surface gradient must be estimated first before local surface curvature can be recovered.

The sign of the Gaussian curvature alone provides reduced information about local surface curvature. Yet, it can be useful for specific purposes such as segmentation. Methods to recover the sign of the Gaussian curvature are described in [2]–[5].

Wolff and Fan [2] recover the sign of the local Gaussian curvature from three images acquired under different conditions of illumination. Estimates of the local surface gradient and precise knowledge of the light source directions are not required. At the same time, Lambertian reflectance is assumed and one of the light source directions must be aligned with the viewing direction.

Okatani and Deguchi [3] recover the sign of the local Gaussian curvature from the sign of the determinant of the 3×3 matrix of image irradiances sampled in each of three images at three distinct local image points. Again, the three images are acquired under different illumination conditions. The method does not need precise information about the light source directions. It is applicable when surface reflectance is diffuse.

Angelopoulou and Wolff [4] recover the sign of the Gaussian curvature directly from three images acquired using illumination from three different light source directions. The method determines the sign of the Gaussian curvature by examining the orientation of a closed curve around each local target point. Again, it is applicable when surface reflectance is diffuse.

Previously, the current authors [5] developed a method to classify six types of local surface curvature. The method was based on an implementation of three light source photometric stereo where reflectance was estimated empirically using a calibration sphere. In this implementation, the required mapping from local five pixel neighborhoods to curvature type was embodied in a radial basis function (RBF) neural network.

Using more than three images has two potential advantages. First, the accuracy of estimation of the sign of the local Gaussian curvature can be improved. Second, shadows and areas of specularity can be overcome. Thus, estimation can be more robust since curvature information can be recovered for a larger region of the visible surface. Previous approaches, [2]–[4], have been limited to three images. The empirical approach [5] has been extended to classify local surface curvature using more than three images [6]. But, the methods of [5], [6] do need a calibration sphere because explicit estimation of the gradient (i.e., surface normal) still is required. On the other hand, [3] and [4] show that the sign of Gaussian curvature can be recovered

Manuscript received February 19, 2001.
Manuscript revised June 20, 2001.

[†]The authors are with the Graduate School of Engineering, Nagoya Institute of Technology, Nagoya-shi, 466-8555 Japan.
[††]The author is with the Department of Computer Science, University of British Columbia, Vancouver, BC, Canada V6T 1Z4.

for diffuse surfaces without estimation of the gradient.

This paper proposes a new method to recover the sign of the Gaussian curvature directly from multiple (more than three) shading images without estimation of the gradient [7]. We use Principal Components Analysis (PCA) to reduce the dimensionality of the original input space and propose a robust algorithm to recover the sign of the local Gaussian curvature from a reduced two-dimensional subspace. The method determines the sign of the local Gaussian curvature at a point by comparing the relative orientation of measurements obtained from the neighbors of that point to the orientation of those measurements when projected onto the two-dimensional subspace. The method can easily make use of many more than three images since, following projection, the curvature estimation problem is 2-D. Finally, the method is extended to show that the sign of the local Gaussian curvature still can be estimated in the presence of specularity given that a pixel with specularity is detected and given that other images of that pixel without specularity remain to support the estimation. Results are demonstrated by experiments on synthetic and real image data.

2. Background

2.1 Sign of the Gaussian Curvature

Let the object surface be given by $z = f(x, y)$. The sign of the Gaussian curvature is the sign of $p_x(x, y)q_y(x, y) - p_y(x, y)q_x(x, y)$, where p and q are the first partial derivatives of z with respect to x and y and p_x, p_y, q_x, q_y are the corresponding second partial derivatives. In the discrete case, we estimate the sign of the Gaussian curvature using a local five point template centered at each discrete point, (x, y).

Let Υ be the standard mapping from the unit surface normal at a point on a smooth object to the associated point on the Gaussian sphere. The orientation of the four neighboring points on the Gaussian sphere under the mapping Υ determines the sign of the Gaussian curvature. If the Gaussian curvature at a point on the object is positive, then its neighbors map to the Gaussian sphere as shown in Fig. 1(a). Conversely, if the Gaussian curvature is negative, then its neighbors appear as shown in Fig. 1(b).

The sign of Gaussian curvature is determined by the relative orientation of the associated points on the Gaussian sphere. The challenge here is to determine the relative orientation of points mapped by Υ without knowing the surface gradient parameters p and q.

2.2 Three-Dimensional Space of Image Irradiances

In the three light source case, let the three irradiance measurements obtained at each pixel be (E_1, E_2, E_3). E_1, E_2 and E_3 can be considered to define the axes of a 3-D right-handed coordinate system. For a Lambertian surface with constant albedo, Woodham [1] showed that a scatter plot of all measurements, (E_1, E_2, E_3), defines a 6-degree-of-freedom ellipsoid. This ellipsoid does not depend on the shape of the object in view nor on the relative orientation between object and viewer. Angelopoulou [4] showed that scatter plots for a variety of diffuse surfaces with constant albedo, including surfaces with varying degrees of surface roughness, remain ellipsoid-like in shape and that the sign of local Gaussian curvature can be determined since the relative orientation of neighboring points in the 3-dimensional space of image irradiances and on the Gaussian sphere is preserved under the Υ mapping.

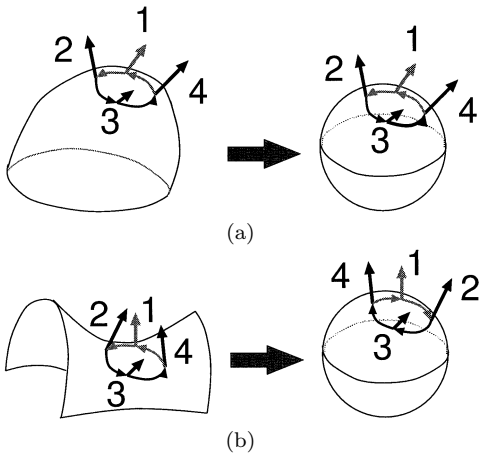

Fig. 1 Mapping onto the Gaussian sphere, (a) positive Gaussian curvature and (b) negative Gaussian curvature.

Angelopoulou [4] also noted that the scatter plot from a surface with multiple distinct albedos consists of multiple distinct ellipsoid-like shapes that differ only in scale as shown in Fig. 2(a). Following [4], we use normalization to remove the effect of varying albedo. Let

$$\boldsymbol{E}' = \left(\frac{E_1}{\|\boldsymbol{E}\|}, \frac{E_2}{\|\boldsymbol{E}\|}, \frac{E_3}{\|\boldsymbol{E}\|} \right) \tag{1}$$

Then, the scatter plot of $\boldsymbol{E}'$ values produces a single, normalized ellipsoid-like shape in (E'_1, E'_2, E'_3) space. Figure 2(b) shows the scatter plot in the 3-dimensional space of normalized image irradiances for a Lambertian sphere with two different albedo values. The sign of the local Gaussian curvature also can be determined in the 3-dimensional space of normalized image irradiances since normalization does not change the direction of the vector $\boldsymbol{E}$. This means normalization preserves the relative orientation of neighboring points. Image irradiance normalization, as defined here, extends in the obvious way to the p image case ($p > 3$).

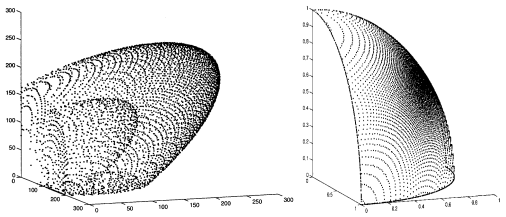

(a) (b)

Fig. 2 Scatter plots synthesized for a Lambertian sphere with 2 albedos, (a) in space of image irradiances and (b) in space of normalized image irradiances.

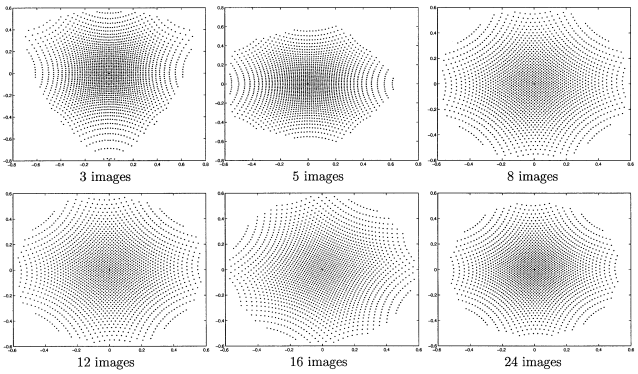

Fig. 3 Eigen plane scatter plots for a Lambertian sphere.

3. Recovering Sign of Gaussian Curvature from a 2-D Subspace

3.1 2-D Subspace of the Space of Normalized Image Irradiances

Assume now the p light source case, where $(p > 3)$. Let the p irradiance measurements obtained at each pixel be denoted by $\boldsymbol{E} = (E_1, E_2, \cdots, E_p)$ and the normalized irradiance vector by $\boldsymbol{E}'$. For given conditions of illumination, viewing and object material, let $\boldsymbol{\Phi}$ be the mapping from a point on the Gaussian sphere to the p-dimensional space of normalized irradiance measurements. For suitably illuminated points, $\boldsymbol{\Phi}$ is invertible since the p-tuple of image irradiances is different for each different surface normal.

We do not attempt to define the relative orientation of four neighboring image points in a p-dimensional space of normalized image irradiances for arbitrary p, $(p > 3)$. Instead, the novel idea is to use Principal Components Analysis (PCA) to reduce the dimensionality of the space of measurements. Each point in the p-dimensional space of normalized irradiances is mapped to a 2-dimensional subspace by a transformation denoted by $\boldsymbol{\Psi}$. $\boldsymbol{\Psi}$ selects the first two principal components of the original p-dimensional space of measurements. We call this 2-dimensional subspace the eigen plane. Example eigen plane scatter plots for a Lambertian sphere with varying number, p, of images are shown in Fig. 3. It is shown that $\boldsymbol{\Psi}$ is a one-to-one mapping that links the relative orientation of points on the Gaussian sphere with that on the eigen plane. Here, relative orientation means the sense, clockwise or counter-clockwise, of the directed curve through a set of locally neighboring points of the given point.

Ignoring second order effects like inter-reflection and shadows, the shape of the scatter plot in the p-dimensional space of normalized irradiances is independent of object shape. The density of various regions of the scatter plot will depend on the actual distribution of surface normals and thus object shape will influence the actual PCA transformation $\boldsymbol{\Psi}$. For a diffusely reflecting surface with the full range of visible surface normals, the scatter plots on the eigen plane will be similar to those shown in Fig. 3. Differences will arise if the distribution of actual surface normals differs substantially from that of a sphere. In some cases, the actual distribution may be narrow. In other cases, scatter plot density normalization may be needed prior to calculating $\boldsymbol{\Psi}$.

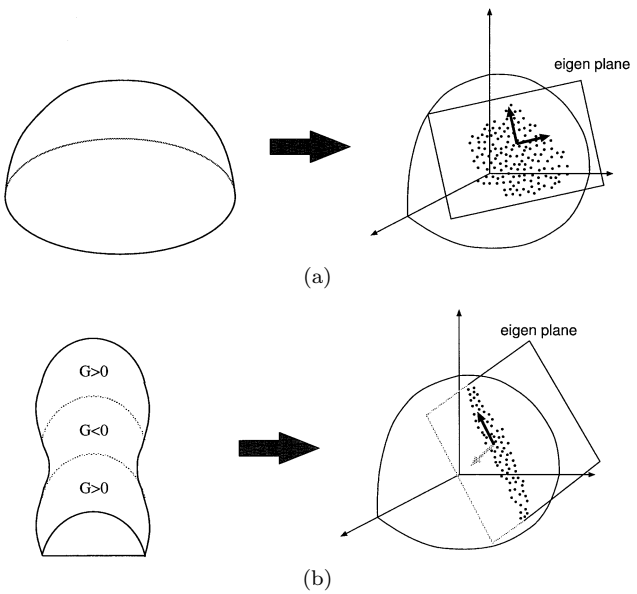

Fig. 4 Eigen plane for $p = 3$, (a) sphere-like object and (b) cylinder-like object.

For the case that the scatter plot in p-dimensional space is similar to that for a sphere, the eigen plane will be almost tangential to the scatter plot of the normalized image irradiances, as shown in Fig. 4(a) (the case of $p = 3$). Conversely, for a cylinder-like object, the scatter plot in the p-dimensional space will have minimal spread and the eigen plane will be almost perpendicular to the the scatter plot of the normalized image irradiances as shown in Fig. 4(b). In this case, the orientation of local image points is not preserved on the eigen plane. Minimal spread of the projected scatter plot on the eigen plane indicates that the method likely will fail. Minimal spread increases the variance of first principal component compared to that of the

second, something that is easy to detect.

Specularity also causes the method to fail because the orientation of local points on the Gaussian sphere generally is not preserved in an area of specularity. The case of non-diffuse surfaces is described in 4.2.2.

3.2 Two Types of Mapping

First, consider the special case of a sphere. Define a local five point image template consisting of a center pixel and its top, bottom, left and right neighbors. Label the pixels as follows: ⓪ is the center point, ① is the top neighbor, and ②, ③ and ④ are the left, bottom and right neighbors respectively (in counter-clockwise order). The corresponding points on the eigen plane will appear either in clockwise or counter-clockwise order. They will appear in the original labelling order if the mapping $\boldsymbol{\Psi} \circ \boldsymbol{\Phi}$ preserves the ordering of points on the sphere. The ordering of points on the eigen plane depends both on the light source arrangement and on $\boldsymbol{\Psi}$.

All coordinate systems are assumed to be the right-handed coordinate systems. To begin the analysis, consider the three light source case. Suppose the three light source directions are arranged in counter-clockwise order with respect to the viewing direction. Then the mapping of local image points to (E_1, E_2, E_3) space preserves the original labelling order [4]. The preservation or reversal of the ordering of points depends explicitly on the ordering of the light sources with respect to the viewing direction. With p light sources, ordering of the corresponding points on the eigen plane also depends on the light source arrangement. Without loss of generality, assume that the light sources are given in counter-clockwise order with respect to the viewing direction (so that discussion about reversals owing to light source ordering can be avoided in the following).

Notwithstanding the above, the projection mapping $\boldsymbol{\Psi}$ may or may not preserve the ordering of the points ① to ④. Let $(\boldsymbol{\psi}_1, \boldsymbol{\psi}_2)$ be the two eigen vectors of the scatter plot covariance matrix that defines $\boldsymbol{\Psi}$. Four combinations exist for the assignment of directions to $\boldsymbol{\psi}_1$ and $\boldsymbol{\psi}_2$. Both $\boldsymbol{\psi}_i$ and $-\boldsymbol{\psi}_i\,(i = 1, 2)$ are possible candidates. Preservation or reversal of the labelling order depends on the particular choice of the directions of $\boldsymbol{\psi}_1$ and $\boldsymbol{\psi}_2$. However, if the eigen plane is defined as a right-handed 2-D coordinate system, $\boldsymbol{\Psi}$ is one of only two types of mapping.

When $\boldsymbol{\Psi}$ preserves the ordering of the four points ① to ④, we call it a "preservation mapping." When $\boldsymbol{\Psi}$ reverses the ordering, we call it a "reversal mapping." For a given imaging situation, it is simple to test whether $\boldsymbol{\Psi}$ defines a preservation or a reversal mapping. Let $\boldsymbol{e}_1, \boldsymbol{e}_2, \cdots, \boldsymbol{e}_p$ be $(1, 0, \cdots, 0)^T$, $(0, 1, 0, \cdots, 0)^T$, $\cdots$, $(0, 0, \cdots, 1)^T$ respectively. Suppose $\boldsymbol{\Psi}$ maps $\boldsymbol{e}_1, \boldsymbol{e}_2, \cdots, \boldsymbol{e}_p$ to $\boldsymbol{e}_1^{'}, \boldsymbol{e}_2^{'}, \cdots, \boldsymbol{e}_p^{'}$ respectively. The distribution of $\boldsymbol{e}_1^{'}, \boldsymbol{e}_2^{'}, \cdots, \boldsymbol{e}_p^{'}$ determines whether $\boldsymbol{\Psi}$ is a preservation or a reversal mapping. $\boldsymbol{\Psi}$ becomes a preservation mapping if $\boldsymbol{e}_1^{'}, \boldsymbol{e}_2^{'}, \cdots, \boldsymbol{e}_p^{'}$ appear in counter-clockwise order. Conversely, $\boldsymbol{\Psi}$ becomes a reversal mapping if they appear in clockwise order. (ASIDE: if the light sources are given in clockwise order then the sense is simply reversed. That is, $\boldsymbol{\Psi}$ is preservation if $\boldsymbol{e}_1^{'}, \boldsymbol{e}_2^{'}, \cdots, \boldsymbol{e}_p^{'}$ appear in clockwise order and reversal if they appear in counter-clockwise order.)

Table 1 Determining the sign of the Gaussian curvature from the orientation of points on the eigen plane.

ordering on the eigen plane	$\boldsymbol{\Psi}$	
	preservation	reversal
counter-clockwise	$G > 0$	$G < 0$
line or a point	$G = 0$	$G = 0$
clockwise	$G < 0$	$G > 0$

For a diffusely reflecting surface with the full range of visible surface normals, the scatter plots on the eigen plane will be similar to those for the sphere. Again, there are two types of mapping. A preservation mapping can be distinguished from a reversal mapping by the ordering of the projections of $\boldsymbol{e}_1^{'}, \boldsymbol{e}_2^{'}, \cdots, \boldsymbol{e}_p^{'}$ onto the eigen plane.

Once $\boldsymbol{\Psi}$ is determined to be a preservation or a reversal mapping, then the sign of the local Gaussian curvature can be recovered as described next.

3.3 Procedure

Table 1 summarizes how to recover the sign of the local Gaussian curvature from the projection of the local image template on the eigen plane. As before, let the five local points on the image be labeled ⓪ for the center point, ① for the top neighbor, ②, ③ and ④ for the other three neighbors oriented counter-clockwise. Suppose $\boldsymbol{\Psi}$ is a preservation mapping. If ① to ④ map onto the eigen plane in a counter-clockwise orientation then $G > 0$. If ① to ④ map in a clockwise orientation then $G < 0$. Conversely, if $\boldsymbol{\Psi}$ is a reversal mapping then the sign simply is the reverse of the above. Should ① to ④ map to a line or to a point on the eigen plane then $G = 0$, regardless of the sense of $\boldsymbol{\Psi}$.

4. Experiments

4.1 Simulated Examples

We use a 2-D sinc function (Eq. (2)) as a test surface. Lambertian reflectance is assumed and eight light source directions are used. Each image is synthesized under the condition that the zenith angle of the direction of illumination is 18 [deg]. One of the eight synthesized images is shown in Fig. 5(a). Each image is 512×512 pixels and gray levels are quantized to 8-bits. The albedo (i.e., the constant parameter C in the im-

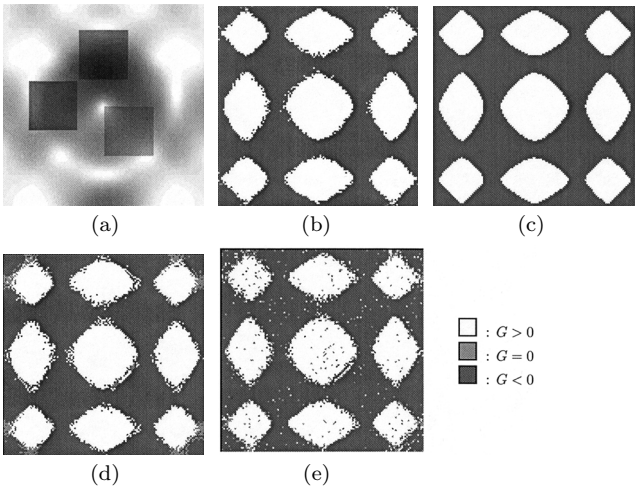

Fig. 5 (a) Synthetic image (b) estimated result (c) theoretical result (d) result by [3] and (e) result by [4].

Table 2 Accuracy with different numbers of light source.

Number of light source	4	6	8	12	16
Accuracy (%)	95.8	96.5	97.1	97.7	98.0

age irradiance equation $E = C\cos(i)^{\dagger}$) takes on two values, $C = 255$ and $C = 150$ (where the square regions in Fig. 5(a) correspond to areas with $C = 150$).

$$f(x,y) = 3 \cdot \frac{\sin(x)}{x} \cdot \frac{\sin(y)}{y} \quad (-2\pi < x, y < 2\pi) \quad (2)$$

The estimated result is shown in Fig. 5(b). Here, the four neighboring points are the four pixels edge adjacent to the center pixel. Figure 5(c) shows the correct result calculated theoretically for comparison purposes. The accuracy of the estimated result is 97.1%. As is evident, the varying albedo is handled correctly. The 2.9% error occurs at the boundary between positive and negative Gaussian curvature (i.e., where G is near zero). Image irradiances obtained around points of zero Gaussian curvature map to nearby locations in the eigen plane. This can cause the method to estimate the sign of G incorrectly.

Table 2 gives the accuracy obtained for different numbers of light sources. Accuracy improves as the number of light sources, and therefore the number of images, increases.

We also compared our method with the two other methods given in [3] and [4]. Both other methods use three light sources only. For the comparison, each image is synthesized under the condition that the zenith angle of the direction of illumination is 18 [deg]. Figure 5(d) shows the result of method [3] and Fig. 5(e) shows that of [4]. Accuracy is 92.4% and 91.6% respectively. Recall that the accuracy for our method using all eight images (Fig. 5(b)) is 97.1%.

Next, two examples of nearly cylindrical objects are used to explore the limitation of the method. As

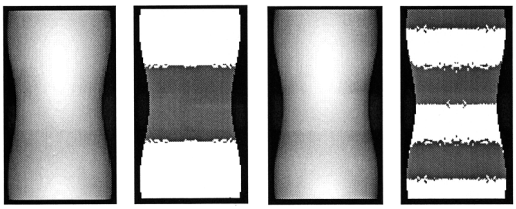

Fig. 6 Synthesized images and results, (a) the correct sign of G is obtained(surface is $z = \sqrt{(2+0.21\sin(x))^2 - y^2}$) and (b) the correct sign of G is not obtained(surface is $z = \sqrt{(2+0.2\sin(x))^2 - y^2}$).

before, eight images are used and each image is synthesized under the condition that the zenith angle of the illuminating direction is 18 [deg]. Examples of the eight synthesized images and experimental results are shown in Fig. 6.

Of course, a true cylinder has $G = 0$ everywhere. For Fig. 6(a), the variance of the second principal component is 3.89% that of the first. For Fig. 6(b), it is only 3.67%. Success or failure depends on the actual conditions of imaging including the number of images, the light source arrangement, quantization and other noise effects. We tested various numbers and arrangements of light sources and various test objects synthetically. Empirically, the method estimates the sign of G correctly when the variance of the second principal component is at least 5% that of the first principal component.

4.2 Real Examples

4.2.1 Diffuse Surfaces

A pottery doll is used for experiments on real data. Fifteen light source directions are used. Images are acquired for two different zenith angles of illumination, eight with a zenith angle of 12 [deg] and seven with a zenith angle of 17 [deg]. Three different test poses of the doll are shown in Fig. 7(a). Measurement conditions for each pose are the same. Each image is 512×512 pixels with 8-bit gray levels. The four neighboring points are the four edge adjacent pixels, as was the case in the simulated examples.

The estimated results are shown in Fig. 7. Figure 7(b) shows the results using only 7 images and Fig. 7(c) shows the results for all 15 images. In this case, the correct result is not known since we have no accurate model of object shape. Qualitatively, the estimated sign of Gaussian curvature appears correct and robust. Figure 7 also demonstrates that the result is viewpoint invariant (i.e., independent of pose). The method estimates results for almost the entire visible surface.

Next, a pottery deer with varying albedo is tested.

$^{\dagger}i$ is the incident angle.

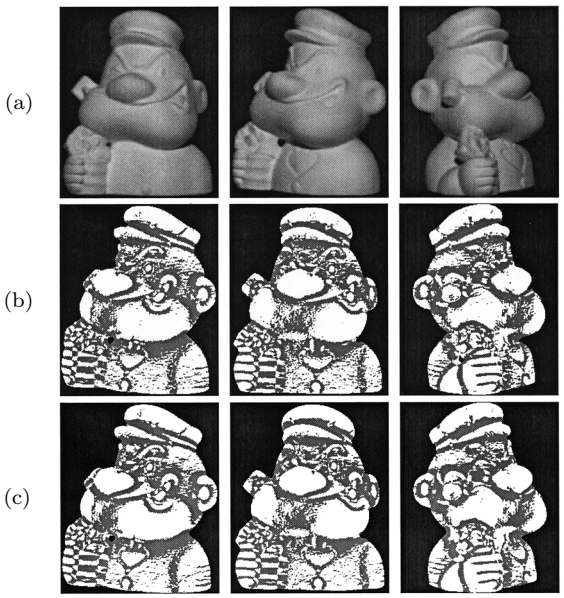

Fig. 7 (a) Real images (b) results (7 images) (c) results (15 images).

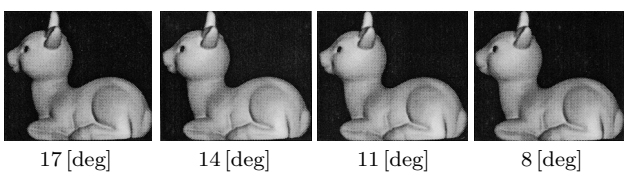

Fig. 8 Example real images.

To test robustness under different conditions of illumination, image sets with different zenith angles (8 [deg] – 17 [deg]) are included. Each image set contains 15 images. Example images are shown in Fig. 8.

Results are shown in Fig. 9(a). With our method, the estimated sign of Gaussian curvature appears qualitatively correct for all image sets, and varying albedo is handled correctly. The results for image sets with zenith angles of are 11, 14 and 17[deg] are of almost identical quality.

Again, we compare our method to that of others. Figure 9(b) shows results for the method of [3]. Figure 9(c) shows results for that of [4]. Both [3] and [4] use three images only. In contrast to our results, the results of these two other methods degrade when the directions of the light sources are more closely aligned. Close alignment of light source directions does result in images that are highly correlated. But, PCA is effective in these circumstances leading to robust estimation nevertheless. This point is one key advantage compared to other methods.

However, all methods are improved by signal averaging. That is, multiple images can be acquired for each condition of illumination that then are summed together to form a single image with improved signal-to-noise ratio. Improvement based on this technique is shown in Figs. 10(b) and (c) (zenith angle is 8 [deg] and each image is made by summing five images acquired in each of the three light source configurations). The results by the method of [3] now are similar to those of our original method. But, our results also can be improved in the same way, as shown in Fig. 10(a). The result of our method remains better than that of the other two.

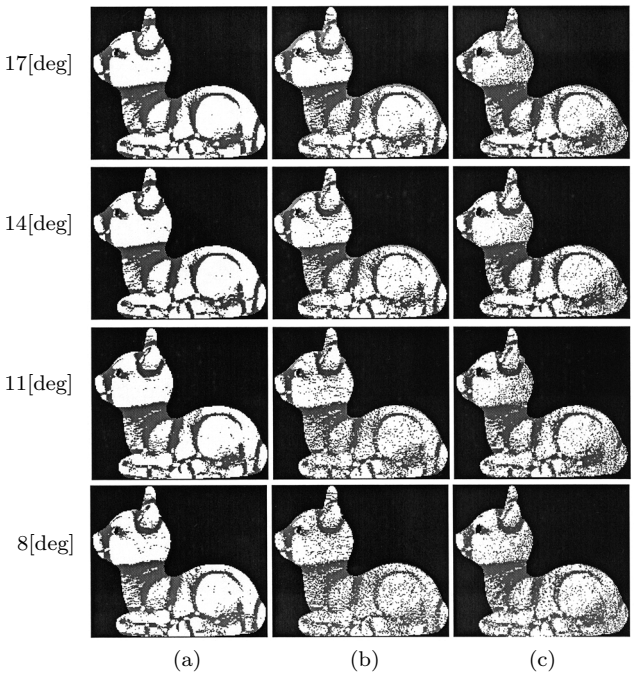

Fig. 9 (a) Our results, (b) results by the method of [3] and (c) results by the method of [4].

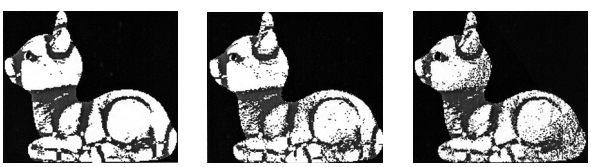

Fig. 10 (a) Our results, (b) results by the method of [3] and (c) results by the method of [4].

Computational cost also is a factor to consider. The method of [3] is the simplest of the three methods considered and therefore is the fastest. The method of [4] is the most complex of the three and therefore is the slowest.

4.2.2 Non-Diffuse Surfaces

A white colored glass is used as another test object. The glass has significant specular reflectance. Experimental conditions are identical to those for the example shown in Fig. 7. Example images are shown in Fig. 11.

We assume constant albedo for the non-specular

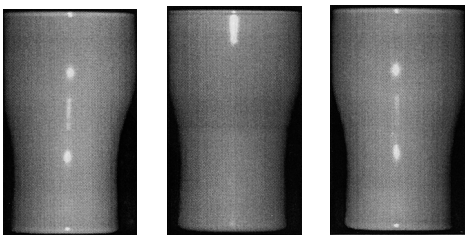

Fig. 11 Real images.

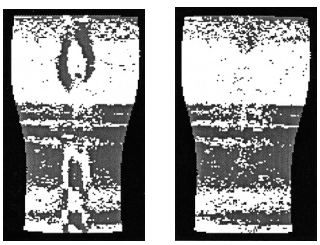

(a) (b)

Fig. 12 (a)Result without removal of specularity and (b) result with removal of specularity.

component of reflection. Observed points which include specularity (i.e., glossiness) have distinctly higher image irradiance values than other points. A threshold Th is used to judge whether a point includes glossiness. Th is estimated from the image itself. Denote pixel coordinates, (i, j), and the corresponding image irradiance, E, by the triple (i, j, E). Let i, j and E define the axes of a 3-D right-handed coordinate system. After all points on the image are plotted in this 3-D space, Th is estimated by checking for peaks in the scatter plot. In this current example, Th is set to be about 180. After Th is chosen, glossy areas can be detected in each image as those areas where image irradiance is greater than Th. At each pixel, (i, j), only the subset of images with image irradiance less than Th are used to estimate the sign of the local Gaussian curvature.

Results are shown in Fig. 12(a) and Fig. 12(b). Comparison of Fig. 12(a) and Fig. 12(b) shows that another benefit of multiple ($p > 3$) images is that glossy areas can be detected (and ignored) with sufficient images still remaining to estimate the sign of the local Gaussian curvature.

The idea to sub-select points in three images with no specularity given a greater number of images can be applied to the other methods too. The challenge, as it is here, is knowing how to select three suitable images from multiple images without specific knowledge of the light source directions or the surface gradients. The selection needs to be dynamic since it varies from point to point. Work to remove the effect of specular reflection in a four image configuration has been reported previously [8], [9]. Dealing with an even larger number of images has the advantage of increasing the opportunity to find a suitable subset to use for each object point.

For further evaluation, the observed image irradiances for the glass object are fit to the Phong reflectance model (Eq. (3)) and estimates made of the parameters s and n.

$$E = C\{s \cdot (2\cos(i)\cos(e) - \cos(g))^n + (1-s)\cos(i)\} \quad (3)$$

where i, e and g are the incident, emittance and phase angles respectively. Parameter n represents the width (i.e., sharpness) of the specular peak. Parameter s represents the relative strength of the specular component compared to that of the diffuse component. Parameter C is an albedo-like term. The estimated results are $s = 0.18$ and $n = 43$.

Again, the 2-D sinc function (Eq. (2)) is used to evaluate accuracy by simulation. Images are synthesized assuming Phong reflectance with $s = 0.18$ and $n = 43$. Measurement conditions are the same as those for the examples in Fig. 11. The accuracy for this example is 96.7%. Further, from an investigation of various combinations of the parameters s and n, it appears that the method can maintain accuracy above 90% whenever $s <= 0.3$. (The method is not sensitive to changes in the value of n.) The method still requires multiple images of points dominated by diffuse reflectance. This becomes less the case as s increases so that overall accuracy decreases. Although Phong reflectance was used in the evaluation, it should be noted that the method does not assume any specific model for the underlying diffuse surface reflectance.

5. Conclusion

This paper described a new method to recover the sign of local Gaussian curvature directly from multiple shading images. Generic diffuse reflectance is assumed. Principal components analysis is used to reduce a high dimensional problem to one of only two dimensions.

The sign of Gaussian curvature is obtained by comparing the relative orientation of five local test points in the image to that of the same points mapped onto the 2-D eigen plane. This is accomplished without any specific model of diffuse surface reflectance or specific information about the direction of the light sources. Previous approaches used three light sources. Here, a larger number of light sources (and therefore a larger number of images) are used. Increased accuracy and robustness have been demonstrated, even when the light source directions are not widely dispersed. Spatially varying albedo also is handled correctly. It also is demonstrated that the method is applicable to glossy surfaces by subselection of images at each point where gloss is detected. Limits of the method are shown by simulation.

In future work, the goal is to enhance the applicability of the method and to explore if the magnitude as well as the sign of the Gaussian curvature can be determined in similar fashion.

Acknowledgment

Major support for Woodham's research is provided by the IRIS Network of Centres of Excellence and by the Natural Sciences and Engineering Research Council of Canada. The authors would like to thank the reviewers for their useful comments.

References

[1] R.J. Woodham, "Gradient and curvature from the photometric-stereo method, including local confidence estimation," J. Opt. Soc. Am. A, pp.3050–3067, Nov. 1994.
[2] L.B. Wolff and J. Fan, "Segmentation of surface curvature using a photometric invariant," Proc. CVPR 1994, pp.23–30, 1994.
[3] T. Okatani and K. Deguchi, "Determination of sign of Gaussian curvature of surface from photometric data," Trans. IPSJ, vol.39, no.5, pp.1965–1972, June 1998.
[4] E. Angelopoulou and L.B. Wolff, "Sign of Gaussian curvature from curve orientation in photometric space," IEEE Trans. PAMI, vol.20, no.10, pp.1056–1066, Oct. 1998.
[5] Y. Iwahori, S. Fukui, R.J. Woodham, and A. Iwata, "Classification of surface curvature from shading images using neural network," IEICE Trans. Inf. & Syst., vol.E81-D, no.8, pp.889–900, Aug. 1998.
[6] S. Fukui, Y. Iwahori, R.J. Woodham, and A. Iwata, "Classification of surface curvature from shading images using neural network and illumination planning," IEICE Trans., vol.J83-D-II, no.2, pp.610–622, Feb. 2000.
[7] S. Fukui, Y. Iwahori, R.J. Woodham, and A. Iwata, "Sign of Gaussian curvature from eigen plane using principal components analysis," Proc. ICPR 2000, vol.III, pp.807–810, Sept. 2000.
[8] E.N. Coleman, Jr. and R. Jain, "Obtaining 3-dimensional shape of textured and specular surfaces using four source photometry," Computer Graphics and Image Processing, vol.18, pp.309–328, 1982.
[9] A. Shashua, "On photometric issues in 3D visual recognition from a single 2D image," International J. Computer Vision, vol.21, no.1/2, pp.99–122, 1997.

Shinji Fukui received the B.S. degree from Dept. of Intelligence and Computer Science, Faculty of Engineering, Nagoya Institute of Technology in 1996, the M.S. and Ph.D. degree from graduate school of Electrical and Computer Engineering, Nagoya Institute of Technology in 1998 and 2001. His research interests include artificial intelligence, neural network and computer vision. He is a member of the IPSJ and the IIEEJ. E-mail: sfukui@center.nitech.ac.jp

Yuji Iwahori received the B.S. degree from Dept. of Computer Science, Faculty of Engineering, Nagoya Institute of Technology in 1983, the M.S. degree and the Ph.D. degree from Dept. of Electrical and Electronics Engineering, Tokyo Institute of Technology, in 1985 and 1988. He joined Nagoya Institute of Technology as a research associate in 1988 and now he is an associate professor of the Center for Information and Media Studies of the same institute. In the meantime, he joined the Dept. of Computer Science, The University of British Columbia as a visiting professor. His interests include Computational Vision, Neural Network and Pattern Recognition. He is a member of the IEEE Computer Society and Information Processing Society of Japan. E-mail: iwahori@center.nitech.ac.jp

Robert J. Woodham received a B.A. (Honours) in Mathematics from the University of Western Ontario in 1971. He received the S.M. (masters) and E.E. (Electrical Engineer) degrees from the Massachusetts Institute of Technology (MIT) in 1974. He received the Ph.D. degree in Artificial Intelligence from MIT in 1977. He was a post-doctoral research scientist in the MIT AI lab until July, 1978. In August, 1978, he became a faculty member at the University of British Columbia (UBC). From 1984 to 1994, he was a Fellow of the Artificial Intelligence and Robotics program of the Canadian Institute for Advanced Research (CIAR). He is currently Professor and Head of Computer Science at UBC. His principal research interest is computational vision, including shape from shading, photometric stereo, motion and optical flow. E-mail: woodham@cs.ubc.ca

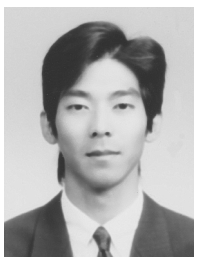

Kenji Funahashi is a research associate in the Center for Information and Media Studies at Nagoya Institute of Technology. His research interests are computer graphics and virtual reality. He received his BE in electronics and information engineering from Gifu University in 1993. He received his ME and Ph.D. in information engineering from Nagoya University in 1995 and 1998. He is a member of VRSJ, and IEEE Computer Society. E-mail: kenji@center.nitech.ac.jp

Akira Iwata is a Professor in the Department of Electrical and Computer Engineering, Nagoya Institute of Technology. He received the B.S., and M.S. and Ph.D. degrees in 1973, 1975, and 1981, receptively, all in Electrical and Electronics Engineering from Faculty of Engineering, Nagoya University, Nagoya, Japan. He was an Alexander Humboldt Foundation Research Fellow at Giessen University, Federal Republic of Germany, in 1982-83. His current interests are in the fields of neural network model, application of neural networks, and medical collaboration system. He is a member of Japanese Neural Network Society, Japan Society of Medical Electronics and Biological Engineering, Information Processing Society of Japan. Professor Iwata received the 1992 Best Paper Award of IEICE (Trans. Inf. & Syst., Vol.J75D-II, no.3, pp.545-553) and the 1997 Best Author Award from IPSJ (J. of IPSJ, Vol.38, No.2, pp.150-154).